Xxxx. Xxx. Xxx. Xxx. AA YYYY 10.1146/((please add article doi))

Abstract

Gusts of moderate and large magnitude induce flow separation and other complexities when they interact with the lifting surfaces of air vehicles. The presence of these *nonlinear gusts* are becoming ubiquitous in twenty-first century air vehicles, where the classic potential flow based methodologies applied in the past may no longer be valid. The parameter space for the presence of large-amplitude gusts is defined, as well as a description of where and when these gusts may primarily be found. Recent research using modern experimental and computational techniques to define the limits of the classical unsteady and indicial aerodynamic theories are summarized, with a focus on discrete transverse, streamwise (longitudinal), and vortex gust encounters. Areas where future research is needed to transition these studies of large-amplitude gust physics to real-time prediction and mitigation during flight are proposed.

Keywords: gusts, nonlinear, separation, transverse, streamwise, vortex

Physics and Modeling of Large Flow Disturbances: Discrete Gust Encounters for Modern Air Vehicles

Anya R. Jones,[1], *Oksan Cetiner*[2], *and Marilyn J. Smith,*[3] [1]*Department of Aerospa*

Contents

1 INTRODUCTION

The era of manned flight began on the morning of December 17, 1903, when the Wright Flyer logged 101.5 seconds in the air over four flights. Unfortunately, a gust of wind soon put an end to the day of testing when it overturned the aircraft and caused severe structural damage (Smithsonian National Air and Space Museum, 1999). In the generations of aircraft designs that have followed, manned flight in clear air has become commonplace. Storms and severe

weather aside, wind gusts and atmospheric turbulence are now considered small disturbances. In the 1990s, however, a rise in micro air vehicle (MAV) research and development led to bird- and insect-scale vehicles that necessarily fly more slowly and carry a lighter payload than larger aircraft (Mueller, 2009). More recently, there has been an uptick in interest in larger unmanned air vehicles (UAVs) for extended intelligence, surveillance, reconnaissance, and delivery and logistics support (Gilday, 2021; Berger, 2020), or as air taxis in urban transport systems (Johnson et al., 2018; Silva et al., 2018). To complete modern UAV missions, vehicles must be capable of executing precise takeoff and landing maneuvers in a constrained airspace. A UAV based on a naval ship, for example, must take off and land on the flight deck without interfering with personnel or other aircraft operations, while a delivery drone or air taxi must be able to perform pick-ups and drop-offs while navigating within an urban environment and in close proximity to people and property.

Advanced Air Mobility (AAM) requires operation in a highly unsteady aerodynamic environment. For a vehicle that must ultimately hover, approach, and land, any atmospheric flow disturbance can become of the same order of magnitude as the flight speed of the vehicle. Current research refers to flow disturbances due to both atmospheric turbulence and shed wakes (e.g., from buildings or ship super structures) as gusts. Thus a gust is simply a flow structure that exists in the environment and causes unsteadiness in the flow about a lifting surface, ultimately resulting in unsteady loading on that surface. In practice, gusts are a combination of many flow structures including shear layers, coherent vortices, updrafts, downdrafts, and turbulence. In the laboratory, it is useful to deconstruct the complex flows observed in flight environments to make the problem more tractable and to highlight the effects of key constituent phenomena. Historically, most studies of gust encounters have focused on small flow disturbances, often motivated by aeroelastic concerns. This review, however, is limited to studies of the incompressible flow about rigid wings and focuses on strong gusts where the magnitude of the gust is similar to that of the vehicle's flight speed.

2 WHERE ARE GUSTS ENCOUNTERED?

2.1 Meteorological Considerations

Most of the large flow disturbances in the atmosphere occur in the Atmospheric Boundary Layer (ABL), illustrated in Figure 1. Strong wind gusts often arise during severe storms and can result in considerable economic and social impact. Meteorologic forecasting of winds has thus been an important topic of research (Sheridan, 2018) and has motivated the type of long-term measurement campaigns necessary for accurate modelling and estimation (Wilczak et al., 2019; Fenerci et al., 2017). The most well-known and commonly used meteorological approach to modelling wind gusts is that of surface-layer gust parameterization. This approach is based on an estimation of the gust factor, i.e., the ratio of the wind gust speed to the mean horizontal wind speed (Durst, 1960). Meteorolog-

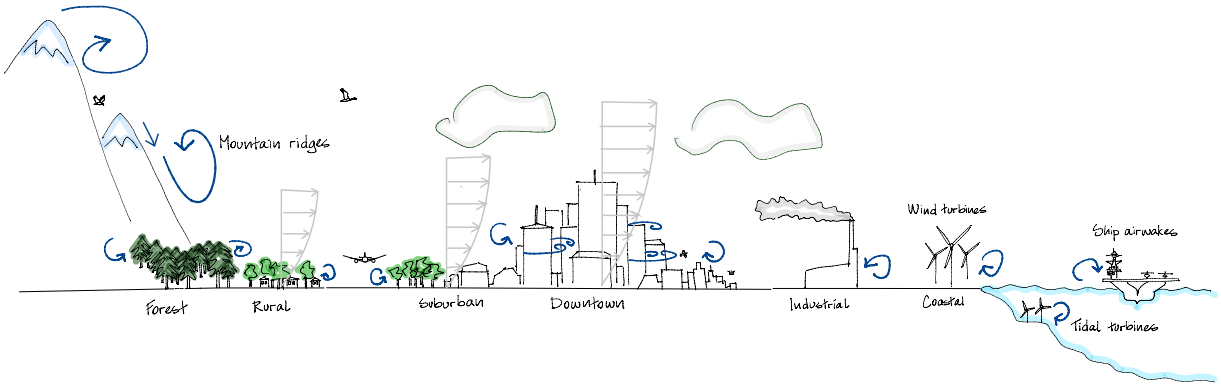

Fig. 1: Gusts in the atmospheric boundary layer (ABL). The ABL thickness grows with increasing roughness from rural areas to suburbs to city centers. Both weather and roughness of the topography play a role in flow separation and shed wakes, and unsteady separated flows are commonly found in many types of terrain including mountain ridges, urban areas, coastal areas, and in the wakes of large structures.

ical data indicate that the scales of unsteady flows in storms can vary widely; updrafts and downdrafts of at least 72 m/s (236 ft/s) have been measured, here with a mean wind speed of 20 m/s for a gust factor of near 3.6 (Nolan et al., 2017; Blanchard, 2013). Similarly, the value of the gust factor is usually on the order of 3 for urban wind comfort assessments, and convective wind gusts in central Europe have gust factors that range between 1–4 (Mohr et al., 2017). A fundamental difference in meteorological concerns and typical aerospace applications, however, is the time scale of interest. Meteorological wind speeds are recorded at a rate of 1–20 Hz and are reported as a time averages over 10 minutes. Wind gusts are defined as the strongest wind measured over 1–3 seconds (Suomi & Vihma, 2018). For fixed structures like buildings and bridges, engineers are most concerned with wind variations over long time scales and the 100 year gust is a reasonable design metric (Peterka & Shahid, 1998). When the primary time scales of relevance are minutes, hours, or years, $\mathcal{O}(10\,\text{Hz})$ is a high time-resolution measurement, but it is of limited relevance to aircraft in motion where the time scale is typically seconds or fractions thereof.

2.2 Air Vehicle Operation

The operational envelope of air vehicles is typically constrained by maximum structural loads, as well as the ability to control the vehicle through any disturbances encountered during flight. Identifying the maximum gust that a vehicle might encounter is thus of utmost importance. The primary challenges in air vehicle operation lie in highly unsteady flows of short time and length scales as these are the most likely to incite large transient airloads. For example, in both

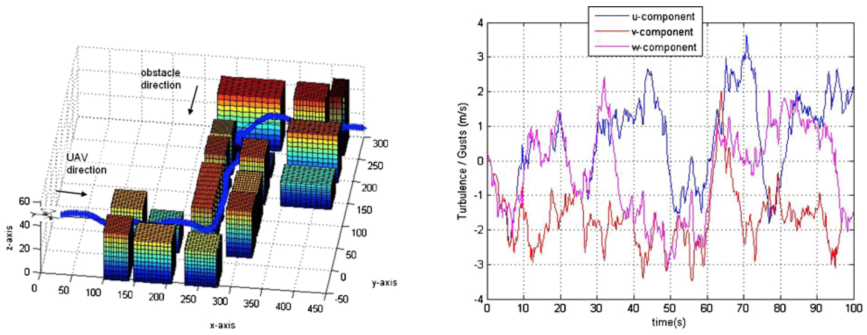

(a) Flight Path (b) Transient velocity profile

Fig. 2: Simulation of UAV flight at 8 m/s through an urban canyon of width 20 m, from Berry et al. (2012). The composition of this simulation is strikingly similar to turbulence measurements by Fenerci et al. (2017). Other work has shown that much higher gust ratios $\mathcal{O}(1)$ can also be encountered in urban environments (Gross, 2014).

search-and-rescue operations in complex terrain (e.g., mountains and canyons) and naval operations from a ship deck, air vehicles must slow to a hover or land in complex air wakes (Dooley et al., 2020a,b; Thedin et al., 2020; Shukla et al., 2019). Naval operations are further complicated by the motion of the ship deck. As on land, there are a wide variety of vehicles that might operate on naval vessels, ranging from reconnaissance UAVs to much larger manned vehicles. One example of a strong gust encounter for a fast manned vehicle is that of burble for an F-15 approaching through the wake of the ship on a carrier-based landing (Cherry & Constantino, 2010). For smaller vehicles, shed vortices from the ship superstructure are also of concern as UAVs are likely to have a mean aerodynamic chord length and stall speed approximately one-tenth that of manned aircraft (Glīzde, 2017). For the same reason, large wind gusts and shear layers will set flight limits for UAVs and MAVs in urban and suburban areas. An example of this environment is shown in Figure 2, where it can be seen that a UAV flying through an urban canyon encounters strong gusts of multiple time scales on all three axes.

3 FUNDAMENTAL FEATURES AND TRADITIONAL MODELING OF GUSTS

3.1 Defining and Parameterizing Gusts

For consistency with the current regulations for vehicle certification or qualification, gusts are described here as either continuous or discrete although atmospheric disturbances consist of both types. Continuous gusts are repre-

sentative of the atmospheric disturbances that arise in clear air turbulence and storms. They are ergodic as defined by Gaussian processes, and are assumed to be isotropic, and stationary in time. Continuous gusts are most commonly evaluated by one of two stochastic models, the Dryden or von Kármán model (Beal, 1993), both of which are comprised of rational power spectral densities that are defined for translational gust velocities in each Cartesian axis.

Discrete gusts, typically of time scales on the order of one convective time, are characterized by their interaction with the vehicle. A discrete gust is an isolated flow structure that may take on several forms, some of which are illustrated in Figure 3a. It may be parameterized as shown in Figure 3b by its magnitude V or gust ratio $GR = V/U_\infty$, and its length or width W. The velocity profile (Fig. 3c) is parameterized by the gust gradient distance, H, which gives the distance over which the gust velocity rises to a maximum. The gust can be one- or two-sided, i.e., the gust gradient distance can describe both an entrance, H_s, and exit, H_e. The shape of a discrete gust can vary and canonical examples include step or top-hat, 1–cosine (one minus cosine), and ramp functions as illustrated in Figure 3c. In recent work, several studies have replicated the 1–cosine gust as a sine-squared profile, which provides the same shape as $\sin^2\theta = (1 - \cos 2\theta)/2$.

3.2 Classic Theories for Discrete Gust Modeling

The classic theories for unsteady aerodynamics and gusts were developed primarily during the first half of the twentieth century for fixed wing flutter or helicopter rotor analysis. While inviscid linear models may vary in their application, they all include the assumptions of thin aerodynamic wings, low angles of attack, and small deflections or motion via the overarching assumption that the flow remains completely attached. On three-dimensional wings, the rate of change of twist along the lifting surface must be small enough that radial or spanwise flow is minimal to maintain local conditions of approximate two-dimensionality and a planar wake that reaches to infinity.

The most inclusive of the many indicial (step) functions applied to transverse gust encounters is Miles's equation (Miles, 1956), which models a gust moving with respect to an airfoil in a constant uniform freestream. The modeling of gusts of arbitrary shapes is achieved via a convolution integral that allows the responses of any number of linear forcing functions to be superimposed (Bisplinghoff et al., 1955). Miles's function introduces a weighting term, λ, that permits the gust velocity to vary so that the gust can move in the same direction and speed as the freestream ($\lambda = 1$), resulting in the classic Küssner stationary gust (Küssner, 1932; Küssner, 1936) in which an airfoil entering a sharp-edged (transverse) gust experiences effective camber (von Kármán & Sears, 1938), and where the circulatory lift can be computed as $c_\ell = 2\pi w_0 \psi(s)/U_\infty$ using the

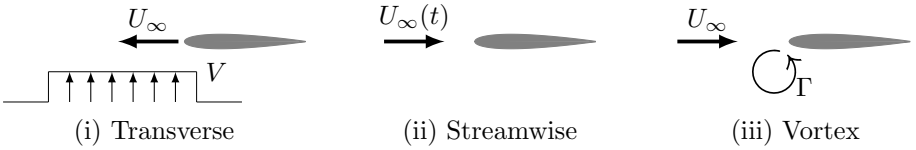

(i) Transverse (ii) Streamwise (iii) Vortex

(a) Three types of discrete gust encounters. Adapted from Jones & Cetiner (2021).

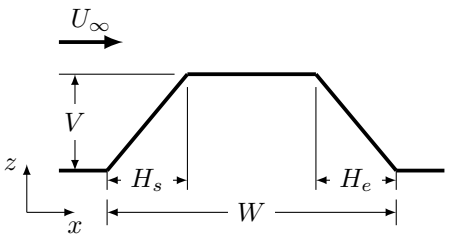

(b) Parameterization of a discrete gust

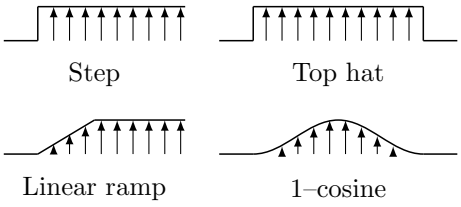

(c) Canonical gust shapes

Fig. 3: Discrete gust encounters. (a) Three types of discrete gust encounters. Each interacts with the wing differently to produce unsteady variations in effective angle of attack and camber. Transverse or normal gusts contain velocities normal to the lifting surface while a streamwise or longitudinal gust adds velocity in the direction of flight. A vortex gust is generated when a coherent vortex interacts with the wing. (b) Parameterization and canonical velocity profiles for discrete transverse gusts. Transverse gusts are primarily parameterized by their gust ratio, $GR = V/U_\infty$, and velocity profile gradient distance, H. (c) Canonical velocity profiles for discrete transverse gusts. Regulations typically refer to 1–cosine gusts, but inviscid theories were derived for sharp-edged gusts.

Küssner function for nondimensional time s, $\psi(s)$:

$$\begin{aligned}\psi(s) &= \frac{1}{2\pi i}\int_{-\infty}^{\infty}\frac{C_g(k)}{k}e^{ik(s-1)}\mathrm{d}k \\ &\approx 1.0 - 0.5e^{-0.13s} - 0.5e^{-s}\end{aligned}$$

Küssner's function $\psi(s)$ is found by integrating across all reduced frequencies k of the modified gust Theodorsen function, $C_g(k) = C(k)[J_o(k) - iJ_1(k)] + iJ_1(k)$, comprised of the Theodorsen function $C(k)$ times Bessel functions applied at the reduced frequency, $k = \omega b/U_\infty$, where $b = 2c$. The gust velocity for a flat plate or thin airfoil is, assuming a small disturbance and angle of attack, estimated as a downwash of $w_0 = -U_\infty\alpha$.

In Miles's problem, if $\lambda = -1$, the gust approaches the airfoil at its trailing edge. When $\lambda = 0$, the result of this model approximates the circulatory lift due to the instantaneous change in angle of attack given by Wagner's function (Wagner, 1925), $c_\ell = -2\pi w_0\phi(s)/U_\infty$:

$$\begin{aligned}\phi(s) &= \frac{1}{2\pi i}\int_{-\infty}^{\infty}\frac{C(k)}{k}e^{iks}\mathrm{d}k \\ &\approx 1.0 - 0.165e^{-0.0455s} - 0.335e^{-0.3s}\end{aligned}$$

For non-zero values of λ, Miles's equation can be applied to model non-stationary gusts that arise from upstream disturbances like those that might be produced by the wake of an upstream body, blade, or vehicle. Recent experimental (Corkery & Babinsky, 2019; Biler et al., 2021; Andreu Angulo et al., 2020) and computational (Grubb et al., 2020; Badrya et al., 2021) investigations have demonstrated that Küssner's model of a stationary gust is sufficient for situations where the gust does not induce large-scale flow separation. At higher gust ratios, the potential flow based Küssner model no longer accurately predicts the aerodynamic response for wide gusts ($\sim 1c$), though it does appear to be sufficient for shorter gusts ($\sim 0.5c$).

Motivated by rotor blades that encounter a periodic freestream over each blade revolution, Isaacs (1945) first introduced modeling of an airfoil at fixed angle of attack in a pulsating freestream. Isaacs (1946) and Greenberg (1947) both extended this model to include sinusoidal variation in pitch. While sinusoidal variations in velocity can be substantial, these theories remain grounded in the typical potential flow assumptions of inviscid, attached flow. Greenberg's formulation is applied most frequently in the literature due to its similarity to the formulation of Theodorsen's equation (1934). The ability to model large variations in velocity lends these theories to large gusts, but the restriction of the wing response to linear aerodynamics must be observed. Granlund et al. (2014) experimentally studied longitudinal gusts for both large and small gust ratios, with and without flow separation. They found that Greenberg's theory was sufficient as long as the flow remained attached, and that the circulatory components were relatively independent of the frequency of motion. However, for large motions at high frequencies, flow separated over the wing and nonlinear

effects such as vortex shedding resulted in augmentation or cancellation of the loading at different frequencies.

Vortex gusts are more complex than their transverse and streamwise counterparts because the passing vortex induces velocities in both the streamwise and transverse directions (§6.3, Fig. 7a). Interaction is inevitable as the vortex approaches the wing, and the separation distance between the vortex and the wing is an important additional parameter. In two dimensions, the induced velocity given by the Biot-Savart law is proportional to the ratio of one over the separation distance, r, squared ($1/r^2$) (Bisplinghoff et al., 1955). Traditionally, the changing velocity induced on a wing as the vortex approached was modeled as superposition of the transverse velocity only. However, these analyses were not physically complete, as the vortex will also induce streamwise velocities, which can also be considered as gusts.

von Kármán & Sears (1938) introduced an approach that models both periodic (sinusoidal) transverse gusts and small arbitrary motions (e.g., uniform, oscillatory, accelerations). Atassi extended this method to include a streamwise velocity component, while maintaining the condition that the flow disturbance must be periodic (Goldstein & Atassi, 1976; Atassi, 1984). When gusts include both velocity components, as in the case of vortex-induced gusts, the influence of camber and angle of attack of the wing can no longer be neglected as they were in similar prior approaches. Young & Smyth (2021) experimentally confirmed that, within the linear regime, the Atassi function is valid for vortex gusts modeled as transverse gusts with a superimposed periodic streawise gust component. One limitation of Atassi's method, however, is that the amplitudes of the vertical and streamwise disturbances are related to their reduced frequencies by the same constant. Thus while Atassi's model (1984) can be used for periodic shed vortices (e.g., in the wake of a bluff body), if both the vertical and streamwise disturbance components are induced by the same vortices, the model is limited to disturbances of equal amplitude.

4 AIRCRAFT REGULATIONS

The gust encounter parameter space for air vehicles is visualized in Figure 4. For the example range of flight vehicles, the extent that their flight envelopes (shaded blue regions) are influenced by the gust gradient distance or velocity is illustrated by the left and right figures, respectively. The higher the flight speed (relative to the gust speed) and longer the chord of the wing, the less influence gusts have, and the less likely it is that gust encounters will be a limiting factor in flight. The lower figures expand the inset regions in the top figures to illustrate the impact gusts have on smaller vehicles. Gust severity is shown by the arrows, and the red shaded region indicates when control of the vehicle is likely to be difficult. It is clear that gusts that are not important for traditional flight vehicles can be critical for modern UAVs.

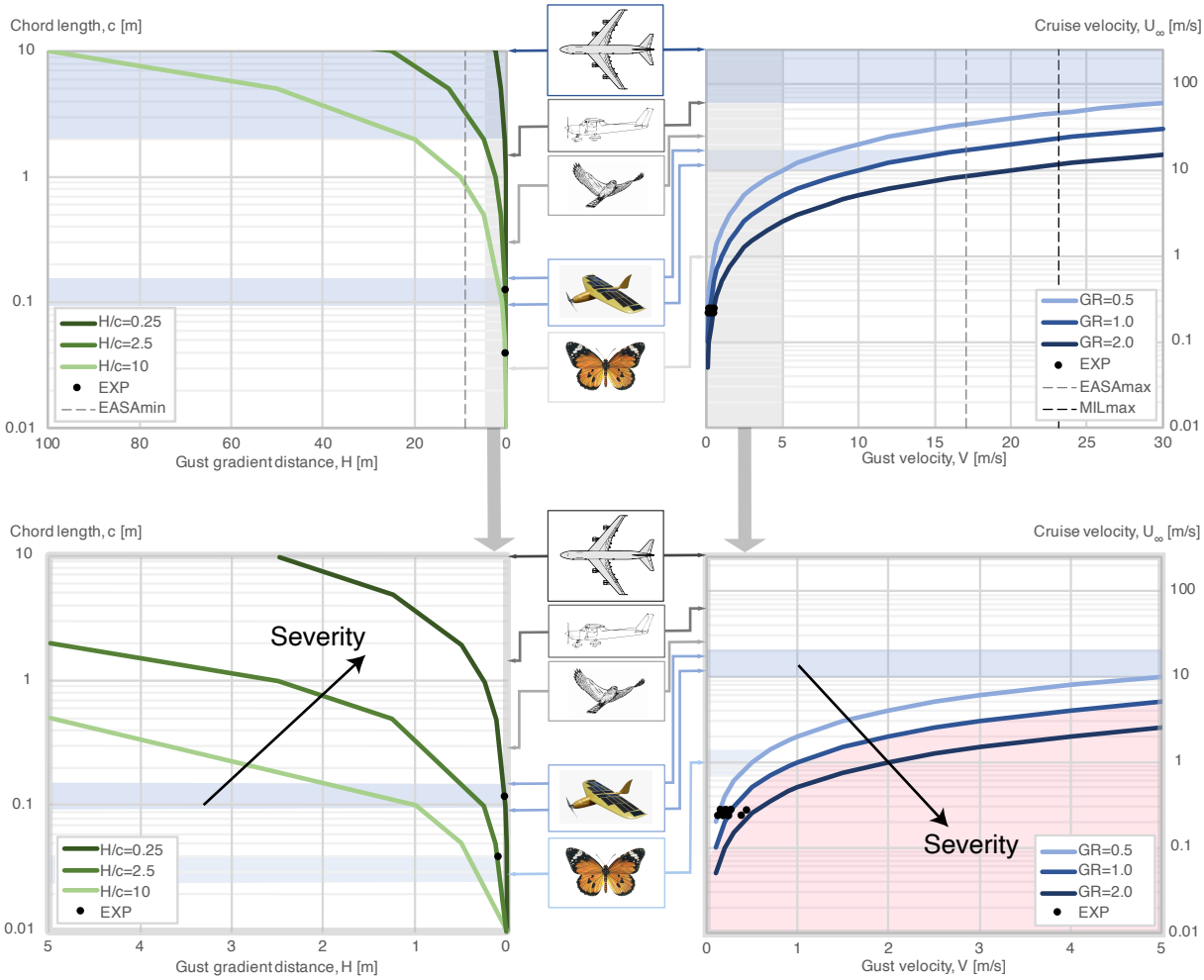

Fig. 4: Gust parameter space. Gust flows are parameterized by their maximum velocity, V, (*right column*) and gradient distance, H, (*left column*). The gust ratio, $GR = V/U_\infty$ relates the gust speed to the flight speed of a sample vehicle, and H/c relates the gust gradient distance to the wing chord. Experimental data (EXP) is from Andreu Angulo et al. (2020) and Biler et al. (2021).

4.1 Fixed-Wing Aircraft

Civilian certification and military qualification of aircraft focus on evaluation of the maximum loads on lifting and control surfaces, as well as the ability to recover from representative or canonical discrete gusts. Civilian requirements for certification of commercial vehicles are found in the U.S. FAA regulations FAR Part 25 (Federal Aviation Administration, 2014b) and European EASA CS-25 regulations (European Union Aviation Safety Agency, 2020a). Military specifications such as MIL-F-8785C (US Dept. of Defense, 1980) for piloted airplanes also detail canonical discrete gust shapes. The primary canonical discrete gust is a 1–cosine profile that is analyzed in both the transverse and longitudinal directions on major lifting and control surfaces. MIL-F-8785C also allows the evaluation of gusts using canonical step-function and linear-ramp formulations.

EASA's CS-25 (European Union Aviation Safety Agency, 2020a) for transport aircraft considers discrete gusts that are either vertical or longitudinal (streamwise). Gust velocities are based on a reference gust velocity, a gust alleviation factor that adjusts the gust intensity according to flight altitude, and variations in the gust gradient distance. The maximum gust velocity is assumed to occur once in 70,000 flight hours. The EASA CS-25 regulations cite gust gradient distances of 9–107 m (30–350 feet) to specify the critical loading response. Certification must include gusts applied to the range of design speeds including a maximum gust velocity and the design cruise speed, and gust velocities should vary linearly from 17.07 m/s (56.0 ft/s) at sea level to 13.41 m/s (44 ft/s) at 4,572 m (15,000 ft). Similar rules apply for normal aircraft certification and are outlined in EASA CS-23 (European Union Aviation Safety Agency, 2020b). MIL-F-8785C indicates that the effects of wind shear, turbulence, and gusts may be analyzed separately rather than superimposed, except for "some analysis and pilot simulation" which should include a total environmental representation. The wind speed for a severe gust at 20 feet above the ground (AGL) is defined as 23.15 m/s (76 ft/s) (US Dept. of Defense, 1980).

For flight controls, U.S. MIL-STD-1797A (US Dept. of Defense, 2004) requires rigid-body analysis of a vehicle's response to both discrete and continuous gusts. If the range of disturbance frequencies under analysis corresponds to or is near a structural mode frequency of the vehicle, then the exact distributions of the disturbances rather than canonical forms should be analyzed to exclude potential vehicle resonance. For carrier operations, lateral and longitudinal disturbance components include steady ship-wake disturbance and periodic ship-motion-induced turbulence in addition to atmospheric disturbances, while the vertical disturbance component considers only random free-air turbulence and random ship-wake disturbance.

4.2 Rotorcraft

Gust requirements for civilian rotorcraft, covered in FAA Parts 27.341 and 29.341, respectively, state that vehicle loads must be substantiated for all air-

speeds from hover to 1.1 times the never-exceed speed or dive speed for vertical gusts of 9.1 m/s (30 ft/s) (Federal Aviation Administration, 2010, 2014a, 2016). For this constant gust velocity, the variation in gust ratio decreases from $GR = 5$ at a flight speed of 2 m/s (6.8 ft/s) to $GR = 0.25$ at 35 m/s (114.8 kts). Both the rotor and all control surfaces are assessed at the same speeds. Unlike FAR 25, these gusts are primarily assumed to be sharp-edged (step function) gusts.

While all of these regulations recognize the role that gusts play in both fixed- and rotary-wing vehicle certification and qualification, they have some limitations in current and future aviation missions. Specifically, lower forward flight speeds near the ground result in higher gust ratios and may result in separated flows. In addition, modern air vehicle missions are expanding into zones (e.g., urban canyons) where wind speeds associated with transients can be stronger than current discrete gust assumptions at higher altitudes. Current and future flight tests (e.g., Thorpe et al., 2018) are expected to identify and clarify expansion of these requirements.

5 THE STUDY OF NONLINEAR GUSTS

The bulk of previous gust-encounter work has focused on small perturbations to the wind speed, largely motivated by aeroelastic effects, wing flutter, and helicopter analysis. The overarching theme of classical theories is that of small disturbances and potential flow theory. Application of these theories has persisted for over three-quarters of a century, but for many modern vehicles and missions, the underlying assumption of attached flow is likely to be violated in the presence of large gusts. A large gust is therefore defined as one where the disturbance is on the same order of magnitude as the freestream or flight speed of the vehicle, where significant separation and nonlinear effects are likely to occur.

5.1 Experimental Considerations

A laboratory experiment ideally represents a well-controlled and well-characterized flow, but large disturbances are inherently unstable and it is difficult to produce a clean canonical gust flow. Küssner, for example, analytically modeled an inviscid transverse gust where the vertical flow disturbance is a step function, but experiments must contend with viscosity. Transverse gusts can be produced as fixed-width jets in quiescent water tanks and test models towed through the stationary gust flow in a transient gust encounter, but real sharp-edged gusts are defined by shear layers (Corkery et al., 2018) and smooth profiles have vorticity distributed throughout the flow (Perrotta & Jones, 2017; Biler et al., 2019). Nonetheless, with this type of setup, it is relatively straightforward to achieve gust ratios of at least 1.5.

Strong streamwise disturbances can be achieved in water by towing a model with an unsteady motion either in a quiescent fluid (Chowdhury & Ringuette, 2021; Marzanek & Rival, 2019; Mulleners et al., 2017) or in the presence of a

freesteam (Granlund et al., 2016). In many ways, towed-model gust encounters are easier to perform than true gust encounters. Specialized facilities are not generally needed, and very high gust ratios and sharp velocity profiles can be achieved. It should be noted, however, that care must be taken to properly account for the added mass force that arises when a model is driven in an unsteady motion. Furthermore, the moving-model problem is not generally equivalent to the moving-fluid problem as it neglects the process of the wing entering the gust flow, wherein the effective angle of attack varies progressively over the wing chord, a critical phase in transverse or vortex gust encounters.

High gust ratios are very difficult to achieve in air, but Farnsworth et al. (2020) describes a low-speed wind tunnel that can dynamically reduce test section flow speeds by 15–50%, and Young & Smyth (2021) achieved a harmonic flow angle oscillation with a peak-to-peak change in angle of attack of 8°. Wei et al. (2019) generated gusts with peak-to-peak deflection angles of only 4.5°, but used an active turbulence grid that can produce sinusoidal variations in either one or two directions. Another unique setup is that of a cross-flow passage on an unsteady flow wind tunnel so that flow disturbances can be produced in two directions: $\sim$10° of flow deflection in the transverse direction and $\sim$ 10% variation in the freestream direction (He et al., 2021; He & Williams, 2020; Rennie et al., 2019).

Vortex gusts are typically generated via rapid pitch of an upstream wing. Peng & Gregory (2015) and Klein et al. (2016) used this approach in a subsonic wind tunnel. In water tunnels, many different variations of pitching, plunging, heaving, and rotating vortex generators have been used (Harding et al., 2014; Biler et al., 2021; Hufstedler & McKeon, 2019; Engin et al., 2018; Rockwood & Medina, 2020). It typically results in a cleaner flow if the vortex can be generated far upstream, thus avoiding its distortion and premature interaction with the test model. However, diffusion of the vortex limits this distance, especially at low Reynolds numbers where the effects of viscosity are strong and a balance must be struck between a clean inflow and an overly diffuse vortex gust.

5.2 Computational Considerations

Although there are many computational approaches for the evaluation of gusts, it remains challenging to resolve the entire frequency range of both continuous and discrete gusts. The approach for computational assessment has thus been to study continuous and discrete gusts separately using high-fidelity computational aerodynamic solvers, also known as Computational Fluid Dynamics (CFD). The presence of highly separated flows, shear layers, and turbulence requires extremely large meshes and, at minimum, using large-eddy simulations in the wakes and separation regions (Hodara & Smith, 2017; Smith et al., 2011; Liggett & Smith, 2012; Gross, 2014; Mohamed et al., 2015). The influence of higher frequencies superimposed on a discrete gust was evaluated during a computational assessment of experiments on a sharp-edged gust of width equal to 2 wing chord-lengths. The experimental gust, with a gust ratio of 1.0, included higher frequencies from the gust jet. Both this and a canonical top-hat gust

without these higher frequencies were analyzed computationally. Due to the presence of the turbulence, the flowfield shear layer features are different, but no difference in the aerodynamic behavior of the wing was observed (Moushegian et al., 2019; Grubb et al., 2020), suggesting that canonical gusts can be utilized for research, even at higher gust ratios.

The CFD simulation of turbulent spectra similar to that found in continuous gusts has thus far relied primarily on synthetic turbulence or eddy methods. These methods prescribe initial turbulent characteristics as a boundary condition to permit the turbulence to evolve in the computational flow domain. They require a large eddy simulation (LES) or a hybrid unsteady Reynolds-Averaged Navier-Stokes (uRANS) – LES approach for implementation. Synthetic eddy modeling (SEM) applied at the boundaries permits the turbulence to evolve as a superposition of eddies (Jarrin, 2008). Key to these approaches is that the continuous turbulence will develop throughout the flow field and interact with the vehicle. In these models, the turbulent characteristics are highly dependent on the prescribed mean velocity, turbulent kinetic energy, and turbulent length and time scales. These characteristics must be extracted and defined for different scenarios and, while it has been a topic of recent research (Dhamankar & Lyrintzis, 2018), there has been little to characterize them for continuous gusts in urban and other environments. In addition, computational meshes must be sufficient in length to permit the evolution of the turbulence, which, along with the refined mesh scales, can require a high level of computational resources for a single simulation.

The larger disturbance length and time scales of discrete gusts are thus easier to computationally model if they are divorced from the high frequency discrete turbulence (i.e., gusts). Numerical modeling of discrete gusts does, however, require that computational codes include the addition of at least the discrete gust inviscid parameters. This reformulation results in several cross-coupling terms between the original formulation and the disturbance, which are mathematically similar to grid velocity terms. These hybrid expressions can be modeled by adding source terms to the inviscid variable vector, but this approach requires modification to the original solver, which may not be possible. For gust-wing interactions where flow remains attached, there is a finite but negligible effect on the integrated aerodynamic coefficients (Wales et al., 2015; Golubev et al., 2010). When gust ratios become large and separation occurs, these terms can no longer be neglected (Badrya et al., 2021). An overset mesh with dynamic motion can model the moving wing with the stationary gust created via the source terms (Badrya et al., 2021) or via jet boundary conditions (Moushegian et al., 2019). Without source terms (requiring code modification), the gust is modeled by a dual set of jet boundary conditions that provide both an entrance and an exit so that the gust velocity is maintained in the simulation. This may require the computational domain to be truncated to incorporate the jet boundary conditions and a refined mesh to ensure that numerical dissipation does not change the problem. For solvers without overset meshes and access to source code, a new set of jet boundary conditions that translate with respect to the wing has been developed (Moushegian et al., 2019; Grubb et al., 2020).

This approach has been successfully validated with experimental data (Corkery et al., 2018), and the limitations are comparable to the overset method with static jet boundary conditions.

5.3 Modeling Considerations

Given exact results from experiments or computations, it is possible to build and validate lower order models and use these to further explore the parameter space of interest. These models are particularly useful for setups that are difficult to construct experimentally or numerically, and provide the unique ability to explore the underlying physics of a problem in a way that is impossible to do in a physical experiment.

One attractive approach is that of vortex models, where the vorticity in a flow is represented by a series of inviscid vortices. This approach, however, quickly becomes very computationally expensive as more vorticity is shed and more vortices are required in an evolving wake. Darakananda & Eldredge (2019) provide one solution in which vortex sheets (rather than a series of point vortices) are used to model trailing shear layers. Vortex models are particularly powerful because while vortices may be aggregated to reduce expense, the model remains exact for whatever number of vortices remain. One of the challenges in applying vortex models to separated flows, however, lies in how to treat the flow at the separation point. Traditionally, the Kutta condition is used to enforce vorticity shedding at the trailing edge. While it is not immediately obvious that the same condition applies at the leading edge, it is commonly used and does appear to perform well (Manar & Jones, 2019). In reality, however, the rounded leading edge of an airfoil will support some amount of suction due to attached flow. The amount of suction that exists before separation occurs can be characterized by the leading edge suction parameter (LESP) (Ramesh et al., 2014). Attached flow is represented by low values of LESP, but as angle of attack increases and more suction is created, LESP grows to a critical value at which flow separates. If the computed value of LESP at a given point in time is below a known critical value (predetermined by experiments), flow in the model is allowed to remain attached. If the computed value is above the critical value, vorticity is shed.

The original application of LESP was to a pitching wing (Ramesh et al., 2014; He et al., 2020), but it has more recently been used to model the effect of a large flow disturbance, i.e., a gust encounter (Darakananda et al., 2018; Hou et al., 2019). In practical applications, the origin of a gust flow is not known and flow estimation based on limited sensor readings becomes key. Le Provost & Eldredge (2020) provide promising results by assimilating data from sensors to augment a physics-based model to include the effects of physics not otherwise represented, in this case the effect of a flow disturbance. The large-scale flow structures over the wing are clearly visible in the vortex model flowfields, while the effect of the gust is evident only in the behavior of the shed vortices. In a different approach, Hou et al. (2019) used machine learning to establish a relationship between surface pressure measurements, a flow disturbance, and

the angle of attack of a wing in a physics-based model. In this work, flow disturbances were modeled as changes in the critical LESP of the wing, which in turn affects how much vorticity is shed from the leading edge. A vortex model was used to train the algorithm to estimate the LESP and angle-of-attack histories from the surface pressure measurements. This was found to be more accurate and require fewer parameters than other approaches, suggesting that machine learning can be used to aid in building or augmenting models, but it remains important to maintain physics-based models as well.

6 PHYSICS OF LARGE GUSTS

6.1 Transverse Gusts

Recent studies of transverse gusts include both step-function and sine-squared shapes as illustrated in Figure 3c. The focus of these studies has primarily been on gusts approximately two chord-lengths wide and of a gust ratio $\mathcal{O}(1)$, and on wings of aspect ratio between 4 and 8. As the data are being compared to two-dimensional theory, flow analysis is performed near the wing mid-span where the flow has been confirmed to be largely two-dimensional. At low gust ratios, the flow is attached, and there is little vorticity in the flowfield. An example of the lift response and flowfield development at high gust ratio is shown in Figure 5. Vorticity rolls up at the leading edge and begins to separate, forming a leading-edge vortex (LEV) with a region of separated flow on the wing just behind the LEV. As the wing moves through the gust, the LEV and the region of the LEV-induced separation extends towards the trailing edge. The LEV increases in strength, expanse, and velocity as gust ratio increases until full separation is reached as shown in Figure 5b for a gust ratio of 1. At a gust ratio of 1.5, the separated region encompasses almost the entire upper surface of the wing when it is fully immersed in the gust.

Figures 6(a-b) show the comparison of numerical results with Küssner's indicial function for a wing at zero incidence passing through a top-hat gust. The magnitude of the maximum lift coefficient is found to increase with gust ratio, and the lift coefficient from numerical simulations follows the theoretical trends until the onset of separation at gust ratios near 0.5 to 0.75. (The pitching moment coefficient is not shown here, but follows the trend of the lift coefficient.) Küssner's theory states that the maximum lift should occur when the wing exits the gust. Once separation occurs and a distinct LEV is present (Fig. 6c), the location of the maximum lift coefficient moves forward in time in a linear fashion (Bonnet et al., 2021) until the flowfield is fully separated at gust ratios near 0.75 to 1.0. At still higher gust ratios, the occurrence of maximum lift remains at the center of the interaction for gusts of width near $2c$. For a fixed gust ratio of 1, the maximum lift remains centered in the gust interaction for top-hat gusts of widths up to $4c$. Similarly, for a sine-squared gust of fixed gust ratio 0.8, Badrya et al. (2021) found the maximum lift coefficient to remain near the center of the gust encounter for gusts up to $9c$ wide (Fig. 6d).

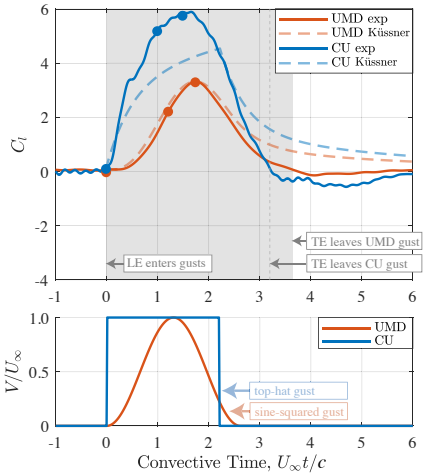

(a) Lift coefficient histories from experimental measurements and analytical results from Küssner's model applied to sine-squared and top-hat gusts.

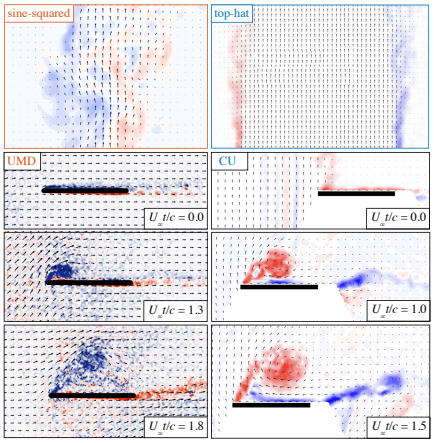

(b) Color contours of vorticity (note inverted colors) overlaid on velocity fields as measured using time-resolved particle image velocimetry measurements of a sine-squared (*left*) and top-hat (*right*) gust encounter.

Fig. 5: Results from a top-hat transverse gust encounter in the University of Cambridge (CU) towing tank and a sine-squared gust encounter in the University of Maryland (UMD) towing tank. Both test models are a flat plate wing at zero incidence passing through a gust of $GR = 1$. From Jones (2020).

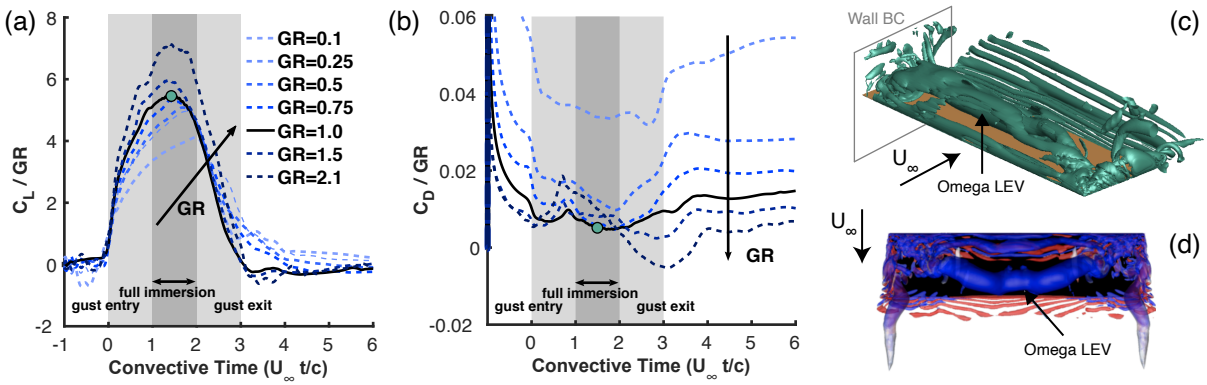

Fig. 6: Computational results for a transverse top-hat (a-c) and sine-squared (d) gust encounter. (a-b) Lift and drag response for increasing gust ratio. (c) Iso-contours of Q-criterion on a wall-bounded semi-span wing in the center of a top-hat gust of width $2c$ and $GR = 1.0$, indicated by the green marker in (b). (d) Iso-contours of Q-criterion colored by vorticity on a finite wing at $U_\infty t/c = 2$ in a sine-squared gust of width $4c$ and $GR = 0.8$. (a-c) from Bonnet et al. (2021); (d) from Badrya et al. (2021).

Drag coefficient (Fig. 6b) is predominately influenced by viscous forces until separation occurs, at which point pressure drag dominates. As gust ratios increase, a peak in drag is observed as the leading edge of the wing enters the gust and decreases until the leading edge exits the gust. At the largest gust ratios, the drag coefficient can decrease to negative values due to recirculation introduced by the interaction of the leading- and trailing-edge vortices (Biler et al., 2019; Bonnet et al., 2021).

While Küssner's model is no longer valid at very high gust ratios for top-hat gusts, it does appear to be valid at higher gust ratios for gusts of smoother shapes where the disturbance velocity grows more slowly over a longer gust gradient distance and remains at a maximum for a shorter period of time. Figure 5 shows experimental force and flowfield measurements for a top-hat gust encounter (CU) and a sine-squared gust encounter (UMD) of similar widths and identical gust ratios of $GR = 1$. In this example, it can be seen that while Küssner's model does not agree particularly well with the experimental results for the top-hat gust, convolution of Küssner's model with the sine-squared gust shape results in close agreement at a gust ratio of 1. The same is true for gust ratios up to at least 1.5 (Andreu Angulo et al., 2020). The formation and shedding of leading- and trailing-edge vortices result in flow nonlinearities (Fig. 5b), but the linear approximation remains relatively valid, at least for first-order estimates. For a short gust (i.e., one of length scale on the order of a chord), the wing begins exiting the gust near the time that the maximum gust magnitude is reached, and thus there is little time for nonlinearities to evolve.

A possible explanation for the excellent agreement with Küssner for smooth

gusts even at high gust ratios is that while Küssner modeled a sharp-edged gust, the model is inviscid and thus does not properly account for the shear layer that exists at the edges of a sharp gust. A smoother gust profile (e.g., sine-squared) has vorticity distributed more evenly throughout the flow and thus there is a slower rise in lift as the wing enters the gust (Andreu Angulo et al., 2020). The two gusts in Figure 5 have the same gust ratio but different velocity profiles and different force curves. If the aerodynamic response of the wing is of primary interest, gust ratio alone is not a sufficient parameterization of the encounter. Minimally, gust gradient distance should also be considered. Furthermore, the flows shown here are for a geometric wing incidence of zero degrees. Linear models do not perform as well if flow over the wing is separated ahead of the gust encounter (e.g., at high angles of attack) (Perrotta & Jones, 2017; Grubb et al., 2020).

6.2 Streamwise Gusts

Streamwise or longitudinal gusts are different from transverse gusts because the flow disturbance does not directly affect the flow angle. Because the flow disturbance is aligned with the freestream, the gust may be quite strong (i.e., of large gust ratio), but the effective angle of attack of the wing remains constant. In this case, changes in lift are due to changes in the local dynamic pressure for small disturbances, but at larger disturbances where separation is predominant, viscous effects become important.

For longitudinal gusts and surging wings, classical theories by Greenberg (1947) and Isaacs (1945, 1946) are typically employed. Granlund et al. (2014) and Kirk & Jones (2019) evaluated longitudinal gusts with respect to Greenberg's theory of oscillating flows for a wide range of gust ratios and wing incidence angles. For attached flows, they verified the applicability of Greenberg's theory, which was found to provide good predictions of both the magnitude and phase of lift. As an offshoot of their studies, Granlund et al. (2014) also confirmed the equivalency of oscillating the flow around a stationary model and oscillating the model in a stationary flow by accounting for buoyancy effects, providing additional freedom in assessing this problem.

In separated flows, significant differences were observed between both the magnitude and phase of experimental measurements and Greenberg's theory (Granlund et al., 2014). While Greenberg's theory predicts a smooth, almost linear increase in the lift amplitude and phase as the reduced frequency ($k = \omega c/2U_\infty$) of oscillation is increased, experimental data indicate a notably different behavior. The observed behavior is similar to Greenberg's prediction near separation, but post-stall behavior differs vastly. Flowfield assessments indicate that these differences are likely due to leading- and trailing-edge vortex interactions, and reduced frequency has a profound impact on this behavior. For wings in large streamwise oscillations where flow fully reverses on the wing, the onset of vortex formation appears to be insensitive to the reduced frequency for $0.1 \leq k \leq 0.3$, where reduced frequency does not play a large role in the development of the near wake (Smith & Jones, 2020). A scaling analysis suggests

that unsteady boundary layer effects are not likely to affect vortex formation while $k < \mathcal{O}(1)$. In this separated flow, linear models must be augmented. A quasi-steady evaluation of the boundary layer equations was found to be sufficient when combined with a shedding criterion based on a critical value of the Falkner–Skan parameter, $\beta = (1/U_e)(\partial U_e/\partial x)$, where U_e is the velocity at the edge of the boundary layer. This provides a promising alternative to LESP for identifying the onset of flow separation and nonlinear flow.

6.3 Vortex Gusts

Vortex gusts are key in many applications, not only for vehicle stability and structural loads, but also for noise. As a vortex passes close to or impinges on a wing, the pressure pulse from the induced velocity can create significant impulsive noise. In particular, rotor blades on vertical lift configurations interact with their own wakes, resulting in vortex gusts due to blade vortex interaction (BVI). BVI is a major area of research for vertical take-off and landing vehicles that have one or more rotors.

Peng & Gregory (2015) categorize vortex interaction in three categories: close interactions, very close interactions, and collisions; characterized by the change in the vortex shape and trajectory near the wing (Fig. 7b). The vortex decays due to pressure gradient (inviscid effects) and shear stress (viscous effects) when it is sufficiently close to the wing's leading edge and boundary layer to interact with them. Linear theories are usually capable of modeling close interactions when separation is avoided and viscous effects on the wing are minimal.

However, in a vortex-wing interaction, a peak in the lift coefficient is observed when the vortex gust impinges on the leading edge of the wing and a counter-rotating leading-edge vortex is formed as shown in Figure 7c. Usually an opposite overshoot is observed when a distinct trailing-edge vortex is formed, followed by the recovery to the steady-state value. As reported in both experimental and numerical studies (Peng & Gregory, 2015; Barnes & Visbal, 2018a), the change in the sense of the impinging vortex reverses the aforementioned loading trend. Comparison of studies conducted at low and high Reynolds numbers (Biler et al. (2021) and Barnes & Visbal (2018b), respectively) indicates that the trend in lift variation is similar and independent of Reynolds number. According to Peng & Gregory (2017), the effect of Reynolds number is revealed in the vortex decay, where a larger impact on pressure load levels is observed at lower Reynolds numbers since the impinging vortex decay rate is inversely proportional to Reynolds number.

Efforts to evaluate classic linear theory to model vortex gusts have largely focused on defining an effective angle of attack with which to estimate the gust strength and lift peak. This approach has been effective, but the optimal definition of location with which to orient the effective angle of attack is still under evaluation (Biler et al., 2021). Comparisons between experiments for sine-squared transverse and vortical gusts for $GR \approx 1$ indicate similar trends in the maximum lift. It should be noted that in these comparisons, the gust

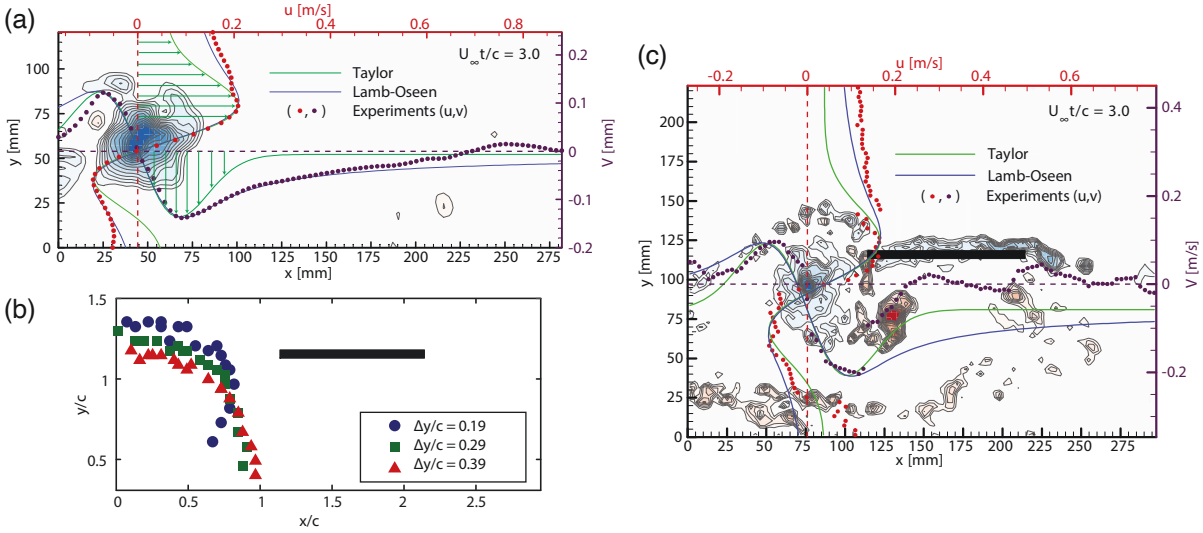

Fig. 7: Vortex gust encounters. (a) Vorticity and velocity profiles of a vortex gust in the absence of the downstream wing. Experimental results and comparison to two theoretical vortex models; data from Engin et al. (2018). (b) Vortex trajectories with the gust generator installed at different heights relative to the wing, $\Delta y/c$. From Biler et al. (2021). (c) Vortex-wing interaction ($\Delta y/c = 0.29$) at maximum lift response; data from Biler et al. (2021)

ratio for the vortex gust was computed using the single peak (half-cycle) rather than peak-to-peak gust velocity values. The lift rise was observed to be higher for the transverse gusts than for the vortex gusts, and lift predictions were accurate for low to moderate gust ratios but deviated at higher gust ratios. Like transverse gusts, large-disturbance vortex gust encounters result in flow separation, nonlinear flow fields, and nonlinear forcing.

6.4 Flow Coupling

There has been much discussion in the research community about the effects of coupling between the gust flow and flow about the lifting surface, especially at high gust ratios. From both experimental and computational observations of transverse gusts, there is an observable deformation in the gusts near the wing at gust ratios of 1.0 and higher that are not observed at lower gust ratios. Corkery & Babinsky (2019) show that deformation of the gust shear layer does not have a large effect on the noncirculatory force on a wing if the wing is a thin flat plate. Gehlert & Babinsky (2021) repeated this analysis for a circular cylinder of finite volume and found that it is necessary to account for body thickness as the bound vorticity requires additional time to evolve after entering the gust, resulting in a different force history. To accurately capture the force history of a thick body passing through a sharp-edged gust, both the thickness and deformation of the bounding shear layer must be accounted for and become more important at higher gust ratios.

In another modern demonstration of a classical theory, Young & Smyth (2021) experimentally demonstrated that, as previously written by Goldstein & Atassi (1976), an incoming gust flow can be linearly superposed to the potential flow about an airfoil. In a clean flow, the inflow velocity is distorted by the presence of the airfoil with increasing distortion following higher wing loading, but is independent of reduced frequency.

Flow coupling is also a major concern for vortex gusts, where the influence of the wing on the upstream flow can be significant (Fig. 7b). In rotary-wing applications, for example, the alignment of a shed vortex with its eventual collision point has a large influence on the blade response, even for small disturbances (De Montaudouin, J. et al., 2014). In a two-dimensional flow where the core of the vortex is aligned with the leading edge of the wing, even inviscid models show the influence of the wing presence on the vortex trajectory. For example, Chen & Jaworski (2020b) revisited analytical point vortex modeling techniques for vortex gusts and compared their results with the experimental work of Peng & Gregory (2015). The potential flow based model accurately predicted the vortex interactions for low and moderate gusts for larger offset distances. For closer interactions, the assumptions of potential flow theory are violated as the vortex path near the wing is influenced by viscous effects in the boundary layer. In viscous flows, other aspects such as viscous vortex–boundary-layer interaction, vortex decay, or viscous vortex–leading-edge interaction enhance the flow coupling in vortex gust encounters (Chen & Jaworski, 2020a).

6.5 Three-Dimensional Gusts

Aircraft regulations and the previous discussion of flow physics have neglected the effects of three-dimensionality, which can be broadly classified as (1) directionality, (2) wing geometry, or (3) gust geometry. For many fixed wing MAVs, the most critical gust would be one that induces a rolling moment on the vehicle (Mohamed et al., 2014; O'Donnell & Mohseni, 2019). Regulations account for directionality with round-the-clock or off-axis gusts, but the underlying physics of large gust encounters may be more complex.

Section 6.3 focused on vortex gusts aligned with the leading edge of the wing such that the flow was essentially two-dimensional (i.e., a parallel vortex), but there are many other types of wing-vortex interactions (Rockwell, 1998). Except for the parallel vortex, these encounters are an inherently three-dimensional problem as vortex alignment and rotation govern the type of instability that arises and affects unsteady wing loading (Barnes et al., 2016). Blade-vortex interactions (BVIs) result in vibratory loading, which can be significantly increased when the vortex orientation is situated along the rotor radius at high forward flight to rotor tip speed ratios (De Montaudouin, J. et al., 2014; Yeo, 2013), resulting in unacceptable flight conditions. Larger-amplitude BVIs can result in separated flows and dynamic stall on the rotor. Interactional aerodynamics, including BVI, is a current topic of research in the vertical lift community (Smith et al., 2020).

Variations in planform and aspect ratio result in complex separated flows that lead to complex wake dynamics and thus complex unsteady wing loading. Some computations have captured this full three-dimensional flow. Top-hat and sine-squared gust encounters of various widths and gust ratios were computed on a wall-mounted semi-span wing (Bonnet et al., 2021) and full-span (Biler et al., 2019) wing. When wing incidence and gust ratio are sufficiently low that flow remains attached, the flowfield consists of regular, almost two-dimensional vorticity shed from the trailing edge of the wing. As separation begins, however, a leading-edge vortex forms and distorts into an omega vortex over the mid-span of the finite wing. Figure 6(c) shows a semi-span model where one end of the wing is anchored at a plane of symmetry, where a distinct corner flow is observed. As the lift is bounded at the wing tips, the LEV forms an Omega vortex, similar to wings in dynamic stall. The Omega vortex is also present on wings modeled at full span, without a plane of symmetry, and is again anchored by the two finite tip vortices as shown in Figure 6(d) for a large-amplitude sine-squared gust encounter.

Whether part of a larger, more complex airwake or atmospheric turbulence, gusts may vary in more than one dimension. For small amplitude but very large-scale gusts with a length much larger than the wing span, a wing acts to filter the effect of spanwise variations in gust strength, thereby decreasing the effective gust strength (Diederich & Drischler, 1957). However, recent modelling efforts have suggested that spanwise-varying harmonic gusts of small amplitude (2.8–3.8%) can result in higher wing loading than their uniform counterparts (Lone & Dussart, 2019). The full effect of multi-dimensional large gust ratios

is an area of current research.

7 MITIGATING GUST RESPONSE

A primary motivation in studying gust encounters is to understand their underlying physics and develop new and effective mitigation strategies. If a gust causes flow separation, it will likely alter the flight path of a low inertia vehicle, but larger UAVs and manned aircraft, especially in hover or approach to landing, are prime candidates for gust rejection systems. Previous work, however, has been limited to small gusts (Heathcote et al., 2018; Al-Battal et al., 2019; Frederick et al., 2010; Heinz et al., 2011; Kerstens et al., 2012).

It is possible to achieve very good gust mitigation results for flow disturbances in the streamwise direction (Chowdhury & Ringuette, 2021). These types of gusts may be the easiest to control because the effective angle of attack of the wing does not change. However, for gusts that are not in-line with the freestream, the effective angle of attack plays a key role in force production. Given an angle of attack, the forces on a maneuvering wing and the effective angle of attack required to negate a known gust can be computed (Sedky et al., 2020; Andreu Angulo & Babinsky, 2021). However, for short-duration nonlinear gusts, the restorative pitch rates are large so that application of active flow control, such as leading- or trailing-edge flaps, is warranted (Young et al., 2016; Frederick et al., 2010; Heinz et al., 2011). The size of the flaps is correlated with response time; larger flaps can generate force more quickly via non-circulatory effects (Mancini et al., 2019), but require more power. Flaps on the leading edge of the wing allow their restoring disturbance to grow while convecting along the wing, increasing the device's effectiveness (Panta et al., 2019). For a gust encounter that is not amenable to an analytical solution, a data-driven model can provide predictions of wing response and recommendations for kinematics to mitigate that response.

During flight, an air vehicle is highly unlikely to have any information about an impending gust encounter, so sensing and prediction are critical. This is a challenging problem as there are multiple relevant time scales including that of the sensor, flow, and actuator. One way to speed reaction times is to avoid the use of model-based control for gust load mitigation. Stochastic models designed via data-driven and machine-learning approaches (e.g., da Silva & Colonius (2018); Le Provost & Eldredge (2020)) may provide good results, but require large representative sets of training data, and results are applicable only within the space over which training has been performed. Even with the use of data-driven models or machine-learning algorithms, analytical models and fundamental understanding of the flow are key and have led to many improvements in numerical simulation performance. Furthermore, while these machine-learning approaches may provide guidance in flow estimation and actuation schedules, rejection of large gusts is likely to require the use of novel actuators that make use of unconventional flow physics (e.g., non-circulatory forcing or added mass). One of the most significant outcomes of recent investigations of high gust ratio

encounters is a more in-depth understanding of their physics: the role that flow separation, shed vorticity, and wake dynamics play; and the time scales over which these flows evolve.

[SUMMARY POINTS]

1. Modern military and civilian missions for small-scale unmanned aerial vehicles (UAVs) and Advanced Air Mobility (AAM) operations in low-level urban environments, nap-of-the-earth, and shipboard operations will encounter gusts on the order of vehicle reference scales with magnitudes that will induce nonlinear, separated flows.

2. Current military and civilian regulations for the U.S. and EU are primarily focused on large-scale aircraft and rotorcraft. While some new regulations are being written for UAVs, the regulations should be revisited to include nonlinear gusts of the anticipated strengths.

3. Recent experimental and computational campaigns using state-of-the-art processes have confirmed the validity of many classical theories for gust encounters where the flow remains attached (i.e., linear potential flow theory). They have also demonstrated that these approaches are not sufficient when the flow separates and the linear assumptions are violated. Significant insight into the complex physics of large-amplitude gust encounters has paved the way for the development of modeling techniques and the study of more complex gust interactions.

4. Linear theories may still provide first-order estimates for large-amplitude discrete gusts with a convective time scale of $\mathcal{O}(1)$ or for smoothly varying gusts where the peak amplitude is of short duration.

5. Transverse gusts have been the focus of most studies; additional research on streamwise and vortex gust encounters is needed to fully characterize the vehicle response parameter space.

[FUTURE ISSUES]

1. Most studies have involved discrete gusts of canonical shapes (e.g., step, ramp, 1–cosine), typically in a single dimension. Research should be expanded to continue in regions of highly complex, three-dimensional gusts, and to include pitching moment and drag responses in addition to lift. Research on gusts in controlled environments is now sufficiently advanced that gust variability observed in actual flight can and should be included, necessitating flight tests and high time-resolution wind measurements.

2. Limited studies indicate that higher frequency turbulence variations of small amplitude, when combined with larger-scale gusts, do not influence the aerodynamic response of a rigid lifting surface. These studies should be expanded to include larger amplitudes of these frequencies, as well as aeroelastic wings and rotors.

3. Nonlinear discrete gusts, by definition, cannot be formally superposed. Additional characterization of nonlinear gusts in multiple directions are required to further understand these limitations. These new studies will aid in determining if stochastic or deterministic approaches can be developed for model-based design and analysis.

4. As the aerodynamics of large gust encounters are highly complex and unsteady, attention to the inclusion of unsteady variations in the form of uncertainty bounds and sensitivities is warranted. This is of particular importance if a data set is to be used for validation. Sensitivity of responses to variables associated with nonlinear gust encounters (gust ratios, gust gradients, etc.) must be well understood if methods to detect large gusts with sufficient time to mitigate them are to be successfully developed.

5. Further study of interactional aerodynamics and aeromechanics is required to quantify the gust response of flexible surfaces and finite wings before nonlinear gust modeling or mitigation strategies can be applied to actual vehicles.

6. While some gust alleviation systems do exist, they have only been applied to small gusts. Can these be extended to large gusts, or is a fundamentally different system needed to meet the response time requirements of these viscous-dominated flows?

7. The use of machine learning and artificial intelligence can aid in understanding these complex flows, while approaches such as surrogate models can aid in the development of reduced-order models. However, future research and engineering should be rooted in fundamental physics to ensure that the conclusions are extensible to different configurations and applications.

Disclosure Statement

The authors are not aware of any biases that might be perceived as affecting the objectivity of this review.

Acknowledgements

The authors gratefully acknowledge support from the U.S. Army Vertical Lift Research Centers of Excellence at the University of Maryland and Georgia Institute of Technology, Cooperative Agreements W911W6-17-2-0004 (A.R.J.) and W911W6-18-2-0002 (M.J.S.); National Science Foundation grants 1553970 and 2003951 (A.R.J.); Office of Naval Research grant N00014-16-1-2731 (M.J.S. and A.R.J.); Army Research Office grants W911NF-13-1-0244 and W911NF-18-1-0291 (M.J.S.); Air Force Office of Scientific Research grant FA9550-16-1-0508 (A.R.J.); and the Applied Vehicle Technology (AVT) Panel of the NATO Science and Technology Organization. The authors would like to especially thank

the members and participants of the NATO-AVT Task Group 282 Unsteady Aerodynamic Response of Rigid Wings in Gust Encounters for their discussions and insights.

References

Al-Battal NH, Cleaver DJ, Gursul I. 2019. Unsteady actuation of counter-flowing wall jets for gust load attenuation. *Aerosp. Sci. Technol.* 89:175–91

Andreu Angulo I, Babinsky H. 2021. Unsteady modelling of pitching wings for gust mitigation. Paper 2021-1999 in AIAA SciTech, Virtual Event, Jan 11–15 & 19–21

Andreu Angulo I, Babinsky H, Biler H, Sedky G, Jones AR. 2020. Effect of transverse gust velocity profiles. *AIAA J.* 58:5123–33

Atassi HM. 1984. The Sears problem for a lifting airfoil revisited – New results. *J. Fluid Mech.* 141:109–22

Badrya C, Biler H, Jones AR, Baeder JD. 2021. Effect of gust width on flat-plate response in large transverse gust. *AIAA J.* 59:49–64

Barnes CJ, Visbal MR. 2018a. Clockwise vortical-gust/airfoil interactions at a transitional Reynolds number. *AIAA J.* 56:3863–74

Barnes CJ, Visbal MR. 2018b. Counterclockwise vortical-gust/airfoil interactions at a transitional Reynolds number. *AIAA J.* 56:2540–52

Barnes CJ, Visbal MR, Huang PG. 2016. On the effects of vertical offset and core structure in streamwise-oriented vortex–wing interactions. *J. Fluid Mech.* 799:128–58

Beal TR. 1993. Digital simulation of atmospheric turbulence for Dryden and von Kármán models. *J. Guid. Control Dyn.* 16:132–38

Berger DH. 2020. Commandant's planning guidance.
`https://www.hqmc.marines.mil/Portals/142/Docs/%2038th%20Commandant%27s%20Planning%20Guidance_2019.pdf?ver=2019-07-16-200152-700`

Berry AJ, Howitt J, Gu DW, Postlethwaite I. 2012. A continuous local motion planning framework for unmanned vehicles in complex environments. *J. Intell. Robot Syst.* 66:477–94

Biler H, Badrya C, Jones AR. 2019. Experimental and computational investigation of transverse gust encounters. *AIAA J.* 57:4608–22

Biler H, Sedky G, Jones AR, Saritas M, Cetiner O. 2021. Experimental investigation of transverse and vortex gust encounters at low Reynolds numbers. *AIAA J.* 59:786–799

Bisplinghoff RL, Ashley H, Halfman RL. 1955. *Aeroelasticity.* Cambridge,MA: Addison-Wesley

Blanchard D. 2013. A Comparison of Wind Speed and Forest Damage Associated with Tornadoes in Northern Arizona. *Weather Forecast.*

Bonnet C, Grubb A, Smith MJ. 2021. *Physics and computational modeling of nonlinear transverse gust encounters.* Work. Pap., Georgia Inst of Tech

Chen H, Jaworski J. 2020a. Aeroelastic encounters of spanwise vortex gusts and the self-rotation of trailing vortices. Paper 2020-0555 in AIAA SciTech, Orlando, FL, Jan 6-10

Chen H, Jaworski JW. 2020b. Aeroelastic interactions and trajectory selection of vortex gusts impinging upon Joukowski airfoils. *J. Fluids Struct.* 96:103026

Cherry BE, Constantino MM. 2010. The burble effect: Superstructure and flight deck effects on carrier air wake. DTIC ADA527798, US Naval Academy, Annapolis, MD

Chowdhury J, Ringuette M. 2021. Effect of a rotating and swept wingtip on streamwise gust alleviation. *AIAA J.* 59:800–11

Corkery SJ, Babinsky H. 2019. An investigation into gust shear layer vorticity and the added mass force for a transverse wing-gust encounter. Paper 2019-1145 in AIAA SciTech, San Diego, CA, Jan 7-11

Corkery SJ, Babinsky H, Harvey JK. 2018. On the development and early observations from a towing tank-based transverse wing-gust encounter test rig. *Exp. Fluids* 59:135

da Silva AFC, Colonius T. 2018. Ensemble-based state estimator for aerodynamic flows. *AIAA J.* 56:2568–78

Darakananda D, da Silva AFdC, Colonius T, Eldredge JD. 2018. Data-assimilated low-order vortex modeling of separated flows. *Phys. Rev. Fluids* 3:124701

Darakananda D, Eldredge J. 2019. A versatile taxonomy of low-dimensional vortex models for unsteady aerodynamics. *J. Fluid Mech.* 858:917–48

De Montaudouin, J., Reveles N, Smith MJ. 2014. Aerodynamic and aeroelastic analysis of rotors at high advance ratios. *Aeronaut. J.* 118:297–313

Dhamankar N. S. BGA, Lyrintzis AS. 2018. Overview of turbulent inflow boundary conditions for large-eddy simulations. *AIAA J.* 56:1317–1334

Diederich FW, Drischler JA. 1957. Effect of spanwise variations in gust intensity on the lift due to atmospheric turbulence. NACA Tech Note 3920, Langley Aeronaut. Lab., Langley Field, VA

Dooley GM, Krebill AF, Martin JE, Buchholz J, Carrica PM. 2020a. Structure of a ship airwake at multiple scales. *AIAA J.* 58:2005–13

Dooley GM, Martin JE, Buchholz J, Carrica PM. 2020b. Ship airwakes in waves and motions and effects on helicopter operation. *Comput. Fluids* 208:104627

Durst C. 1960. Wind speeds over short periods of time. *Meteor. Mag.* 89:181–87

Engin K, Aydin E, Zaloglu B, Fenercioglu I, Cetiner O. 2018. Large scale spanwise periodic vortex gusts or single spanwise vortex impinging on a rectangular wing. Paper 2018-3086 in the 2018 Fluid Dynamics Conference, Atlanta, GA, Jun 25-29

European Union Aviation Safety Agency. 2020a. Certification specifications and acceptable means of compliance for large aeroplanes. EASA-CS-25, EASA, Cologne, Germany

European Union Aviation Safety Agency. 2020b. Certification specifications for normal-category aeroplanes and acceptable means of compliance and guidance material to the certification specifications for normal-category aeroplanes. EASA-CS-23, EASA, Cologne, Germany

Farnsworth J, Sinner D, Gloutak D, Droste L, Bateman D. 2020. Design and qualification of an unsteady low-speed wind tunnel with an upstream louver system. *Exp. Fluids* 61:181

Federal Aviation Administration. 2010. Federal Aviation Regulations: airworthiness standards. FAR Part 29, FAA, Washington, DC

Federal Aviation Administration. 2014a. Advisory Circular, Certification of transport category rotorcraft. AC 29-2C, Chg 6, FAA, Washington, DC

Federal Aviation Administration. 2014b. Advisory Circular, Dynamic gust loads. AC 25.341-1, FAA, Washington, DC

Federal Aviation Administration. 2016. Advisory Circular, Certification of normal category rotorcraft. AC 17-1B, Chg. 7, FAA, Washington, DC

Fenerci A, Øiseth O, Rønnquist A. 2017. Long-term monitoring of wind field characteristics and dynamic response of a long-span suspension bridge in complex terrain. *Eng. Struct.* 147:269–84

Frederick M, Kerrigan EC, Graham JMR. 2010. Gust alleviation using rapidly deployed trailing-edge flaps. *J. Wind Eng. Ind. Aerodyn.* 98:712–23

Gehlert P, Babinsky H. 2021. Noncirculatory Force on a Finite Thickness Body Encountering a Gust. *AIAA J.* 59:719–30

Gilday M. 2021. Chief of Naval Operations (CNO) navigation plan (NAVPLAN). 210111-N-BB269-1001, US Navy Office of Information, Washington, DC.
https://www.navy.mil/Press-Office/Press-Releases/display-pressreleases/Article/2467465/cno-releases-navigation-plan-2021/

Glīzde N. 2017. Plotting the flight envelope of an unmanned aircraft system air vehicle. *Transp Aerospace Eng* 4:80–87

Goldstein ME, Atassi H. 1976. A complete second-order theory for the unsteady flow about an airfoil due to a periodic gust. *J. Fluid Mech.* 74:741–65

Golubev V, Hollenshade T, Nguyen L, Visbal M. 2010. High-accuracy low-Re simulations of airfoil-gust and airfoil-vortex interactions. Paper 2010-4968 in the 40th AIAA Fluid Dynamics Conference and Exhibit, Chicago, IL, Jun 28 – July 1

Granlund K, Monnier B, Ol M, Williams DR. 2014. Airfoil longitudinal gust response in separated vs. attached flows. *Phys. Fluids* 26:027103

Granlund K, Ol MV, Jones AR. 2016. Streamwise oscillation of airfoils into reverse flow. *AIAA J.* 54:1628–36

Greenberg J. 1947. Airfoil in a sinusoidal motion in a pulsating stream. NACA Tech. Note 1326, Langley Aeronaut. Lab., Langley Field, VA

Gross G. 2014. On the estimation of wind comfort in a building environment by micro-scale simulation. *Meteorol. Z.* 23:51–62

Grubb A, Moushegian A, Heathcote D, Smith MJ. 2020. Physics and computational modeling of nonlinear transverse gust encounters. Paper 2020-0080 in AIAA SciTech, Orlando, FL, Jan 6-10

Harding S, Payne G, Bryden I. 2014. Generating controllable velocity fluctuations using twin oscillating hydrofoils: Experimental validation. *J. Fluid Mech.* 750:113–23

He G, Deparday J, Siegel L, Henning A, Mulleners K. 2020. Stall delay and leading-edge suction for a pitching airfoil with trailing-edge flap. *AIAA J.* 58:5146–55

He X, Asztalos K, Henry J, Dawson STM, Williams DR. 2021. Generating traveling cross-flow gusts in a wind tunnel. Paper 2021-1938 in AIAA SciTech, Virtual Event, Jan 11–15 & 19–21

He X, Williams DR. 2020. Spectral feedback control of turbulent spectra in a wind tunnel. *Exp. Fluids* 61:175

Heathcote DJ, Gursul I, Cleaver DJ. 2018. Aerodynamic load alleviation using minitabs. *J. Aircr.* 55:2068–77

Heinz J, Sørensen NN, Zahle F. 2011. Investigation of the load reduction potential of two trailing edge flap controls using CFD. *Wind. Energy* 14:449–62

Hodara J, Smith MJ. 2017. Hybrid Reynolds-Averaged Navier–Stokes/Large-Eddy Simulation closure for separated transitional flows. *AIAA J.* 55:1948–58

Hou W, Darakananda D, Eldredge JD. 2019. Machine-learning-based detection of aerodynamic disturbances using surface pressure measurements. *AIAA J.* 57:5079–93

Hufstedler EAL, McKeon BJ. 2019. Vortical gusts: Experimental generation and interaction with wing. *AIAA J.* 57:921–31

Isaacs R. 1945. Airfoil theory for flows of variable velocity. *J. Aeronaut. Sci.* 12:113–17

Isaacs R. 1946. Airfoil theory for rotary wing aircraft. *J. Aeronaut. Sci.* 13:218–20

Jarrin N. 2008. Synthetic inflow boundary conditions for the numerical simulation of turbulence. Ph.D. thesis

Johnson W, Silva C, Solis E. 2018. Concept vehicles for air taxi operations. Paper presented at the AHS Aeromechanics Design for Transformative Vertical Lift Conference, San Francisco, CA, Jan 16-19

Jones AR. 2020. Gust encounters of rigid wings: Taming the parameter space. *Phys. Rev. Fluids* 5:110513

Jones AR, Cetiner O. 2021. Overview of unsteady aerodynamic response of rigid wings in gust encounters. *AIAA J.* 59:731–36

Kerstens W, Pfeiffer J, Williams D, King R, Colonius T. 2012. Closed-loop control of lift for longitudinal gust suppression at low Reynolds numbers. *AIAA J.* 49:1721–28

Kirk PB, Jones AR. 2019. Vortex formation on surging aerofoils with application to reverse flow modelling. *J. Fluid Mech.* 859:59–88

Klein S, Scholz P, Radespiel R. 2016. Transient, three-dimensional disturbances interacting with a high-lift airfoil-wind tunnel experiments. Paper 2016-1844 in the 54th AIAA Aerospace Sciences Meeting, San Diego, CA, Jan 4-8

Küssner HG. 1932. Stresses produced in airplane wings by gusts. NACA Tech Memo 654, Langley Mem. Aeronaut. Lab., Langley Field, VA

Küssner HG. 1936. Zusammenfassender Bericht über den instationären Auftrieb von Flügeln. *Jahrb. Dtsch. Luftfahrtforsch.* 13:410–24

Le Provost M, Eldredge J. 2020. Ensemble-filtered vortex modeling of strongly disturbed aerodynamic flows arXiv:2008.11309 [Phys.ics.flu–dyn]

Liggett N, Smith MJ. 2012. Temporal convergence criteria for time-accurate viscous simulations of separated flows. *Comp. & Fluids* 66:140–56

Lone M, Dussart G. 2019. Impact of spanwise non-uniform discrete gusts on civil aircraft loads. *Aeronaut. J.* 123:93–120

Manar FH, Jones AR. 2019. Evaluation of potential flow models for unsteady separated flow with respect to Experimental data. *Phys. Rev. Fluids* 4:034702

Mancini P, Medina A, Jones AR. 2019. Experimental and analytical investigation into lift prediction on large trailing edge flaps. *Phys. Fluids* 31:013106

Marzanek MF, Rival DE. 2019. Separation mechanics of non-slender delta wings during streamwise gusts. *J. Fluids Struct.* 90:286–96

Miles JW. 1956. The aerodynamic force on an airfoil in a moving gust. *J. Aeronaut. Sci.* 23:1044–50

Mohamed A, Carrese R, Fletcher D, Watkins S. 2015. Scale-resolving simulation to predict the updraught regions over buildings for MAV orographic lift soaring. *J. Wind Eng. Ind. Aerodyn.* 140:34–48

Mohamed A, Massey K, Watkins S, Clothier R. 2014. The attitude control of fixed-wing MAVS in turbulent environments. *Prog. Aerosp. Sci.* 66:37–48

Mohr S, Kunz M, Richter A, Ruck B. 2017. Statistical characteristics of convective wind gusts in Germany. *Nat. Hazards Earth Syst. Sci.* 17:957–69

Moushegian A, Weston C, Smith MJ. 2019. Analysis of a wing moving through a nonlinear gust. Paper 2019-0637 in the AIAA Fluid Dynamics Conference, San Diego, CA, Jan 7–11

Mueller T. 2009. On the birth of micro air vehicles. *Int. J. Micro Air Veh.* 1:1–12

Mulleners K, Mancini P, Jones AR. 2017. Flow development on a flat-plate wing subjected to a streamwise acceleration. *AIAA J.* 55:2118–22

Nolan DS, Dahl NA, Bryan GH, Rotunno R. 2017. Tornado vortex structure, intensity, and surface wind gusts in large-eddy simulations with fully developed turbulence. *J. Atmos. Sci.* 74:1573–97

O'Donnell R, Mohseni K. 2019. Roll Control of Low-Aspect-Ratio Wings Using Articulated Winglet Control Surfaces. *J. Aircr.* 56:419–30

Panta A, Watkins S, Marino M, Fisher A, Mohamed A. 2019. Lift response of rapidly actuated leading-edge and trailing-edge control surfaces for MAVs. Paper 2019-1397 in AIAA SciTech, San Diego, CA, Jan 7–11

Peng D, Gregory JW. 2015. Vortex dynamics during blade-vortex interactions. *Phys. Fluids* 27:053104

Peng D, Gregory JW. 2017. Asymmetric distributions in pressure/load fluctuation levels during blade-vortex interactions. *J. Fluids Struct.* 68:58–71

Perrotta G, Jones AR. 2017. Unsteady forcing on a flat-plate wing in large transverse gusts. *Exp. Fluids* 58:101

Peterka JA, Shahid S. 1998. Design gust wind speeds in the United States. *J. Struct. Eng.* 124:207–14

Ramesh K, Ramesh K, Gopalarathnam A, Gopalarathnam A, Granlund K, et al. 2014. Discrete-vortex method with novel shedding criterion for unsteady aerofoil flows with intermittent leading-edge vortex shedding. *J. Fluid Mech.* 751:500–38

Rennie R, Catron B, Feroz M, Williams D, He X. 2019. Dynamic behavior and gust simulation in an unsteady flow wind tunnel. *AIAA J.* 57:1423–33

Rockwell D. 1998. Vortex-body interactions. *Ann. Rev. Fluid Mech.* 30:199–229

Rockwood M, Medina A. 2020. Controlled generation of periodic vortical gusts by the rotational oscillation of a circular cylinder and attached plate. *Exp. Fluids* 61:65

Sedky G, Jones AR, Lagor F. 2020. Lift regulation during transverse gust encounters using a modified Goman-Khrabrov model. *AIAA J.* 58:3788–98

Sheridan P. 2018. Current gust forecasting techniques, developments and challenges. *Adv. Sci. Res. Advances* 15:159–72

Shukla S, Sinha SS, Singh SN. 2019. Ship-helo coupled airwake aerodynamics: A comprehensive review. *Prog. Aerosp. Sci.* 106:71–107

Silva C, Johnson W. SE, Patterson M, Antcliff KR. 2018. VTOL urban air mobility concept vehicles for technology development. Paper 2018-3847 in the AIAA Aviation Technology, Integration, and Operations Conference, Atlanta, GA, Jun 25–29

Smith LR, Jones AR. 2020. Vortex formation on a pitching aerofoil at high surging amplitudes. *J. Fluid Mech.* 905:A22

Smith MJ, Gardner AD, Jain R, Peters DA, Richez F. 2020. Rotating wing dynamic stall: State of the art and future directions. In the Proceedings of the VFS 76 Annual Forum, Virtual Event, Oct. 5-8

Smith MJ, Liggett N, Koukol BCG. 2011. The aerodynamics of airfoils at high and reverse angles of attack. *J. Aircr.* 48:2012–23

Smithsonian National Air and Space Museum. 1999. The Wright Flyer: From invention to icon. https://airandspace.si.edu/exhibitions/wright-brothers/online/icon/1903.cfm

Suomi I, Vihma T. 2018. Wind gust measurement techniques – From traditional anemometry to new possibilities. *J. Sensors* 18:1300

Thedin R, Murman SM, Horn J, Schmitz S. 2020. Effects of atmospheric turbulence unsteadiness on ship airwakes and helicopter dynamics. *AIAA J.* 57:534–46

Theodorsen T. 1934. General theory of aerodynamic instability and the mechanism of flutter. NACA Tech Memo 496, Langley Mem. Aeronaut. Lab., Langley Field, VA

Thorpe R, McCrink M, Gregory J. 2018. Measurement of unsteady gusts in an urban wind field using a UAV-based anemometer. Paper 2018-4218 in the 2018 Applied Aerodynamics Conference, Atlanta, GA, Jun 25 – 29

US Dept. of Defense. 1980. Flying qualities of flying airplanes. Military specification MIL-F-8785C, US Dept. of Defense, Washington, DC.

US Dept. of Defense. 2004. Flying qualities of piloted aircraft. MIL-STD-1797A (Notice 3), US Dept. of Defense, Washington, DC

von Kármán T, Sears W. 1938. Airfoil theory for non-uniform motion. *J. Aeronaut. Sci.* 5:379–90

Wagner H. 1925. Uber die entstehung des dynamischen auftriebes von tragflügeln. *Z. Angew. Math. Mech.* 5:17–35

Wales C, Jones D, Gaitonde A. 2015. Prescribed velocity method for simulation of aerofoil gust responses. *J. Aircr.* 52:64–76

Wei NJ, Kissing J, Wester TTB, Wegt S, Schiffmann K, et al. 2019. Insights into the periodic gust response of airfoils. *J. Fluid Mech.* 876:237–63

Wilczak JM, Stoelinga M, Berg LK, Sharp J, Draxl C, et al. 2019. The second wind forecast improvement project (WFIP2): Observational field campaign. *Bulletin of the American Meteorological Society* 100:1701–23

Yeo H. 2013. Investigation of UH-60A rotor performance and loads at high advance ratios. *J. Aircr.* 50:576–89

Young A, Farman J, Miller R. 2016. Load alleviation technology for extending life in tidal turbines. In the Proceedings of Renew 2016, 2nd International Conference on Renewable Energies Offshore, Lisbon, Portugal, Oct. 24-26

Young AM, Smyth ASM. 2021. Gust-airfoil coupling with a loaded airfoil. *AIAA J.* 59:773–85